





Review

High- and Ultra-High-Purity Aluminum, a Review on Technical Production Methodologies

Danilo C. Curtolo [†], Neng Xiong [†], Semiramis Friedrich ^{*,†} and Bernd Friedrich [‡]

IME Institute for Process Metallurgy and Metal Recycling, RWTH Aachen University, Intzestr. 3, 52056 Aachen, Germany; dcurtolo@ime-aachen.de (D.C.C.); nxiong@ime-aachen.de (N.X.); bfriedrich@ime-aachen.de (B.F.)

* Correspondence: sfriedrich@ime-aachen.de; Tel.: +49-0241-80-95977

† These authors contributed equally to this work.

‡ This author is the principal investigator.

Abstract: Aluminum and aluminum-based alloys have been used for many years. In view of the increase in material purity requirements of advanced technology products, research regarding high-purity aluminum has gained significant attention in recent years. In this review, we seek to describe the fundamental purification principles and the mechanisms of various segregation techniques used to produce high-purity aluminum. Moreover, we aim to provide an overview of high-purity aluminum production, with particular emphasis on: (a) principles on how to produce high-purity aluminum by layer- and suspension-based segregation methods; (b) discussion of various influencing process parameters for each technique, including three-layer electrolysis, vacuum distillation, organic electrolysis, suspension-based segregation, zone melting, Pechiney, Cooled Finger, and directional solidification; as well as (c) investigations of fundamental working principles of various segregation methods and corresponding reported end-purification for the production of HP-Al. Eventually, the end-reported product purity, and advantages and disadvantages of various purification methods and technologies are summarized. By analyzing and comparing the characteristics of different methods, we put forward suggestions for realizing efficient and environmentally friendly production of high-purity aluminum in the future.

Keywords: high-purity aluminum; purification; segregation



Citation: Curtolo, D.C.; Xiong, N.; Friedrich, S.; Friedrich, B. High- and Ultra-High-Purity Aluminum, a Review on Technical Production Methodologies. *Metals* **2021**, *11*, 1407. <https://doi.org/10.3390/met11091407>

Academic Editor: Yasar Kocaefe

Received: 5 July 2021

Accepted: 31 August 2021

Published: 6 September 2021

Publisher's Note: MDPI stays neutral with regard to jurisdictional claims in published maps and institutional affiliations.



Copyright: © 2021 by the authors. Licensee MDPI, Basel, Switzerland. This article is an open access article distributed under the terms and conditions of the Creative Commons Attribution (CC BY) license (<https://creativecommons.org/licenses/by/4.0/>).

1. High- and Ultra-High-Purity Aluminum

The primary form of aluminum—from the Hall–Héroult process—has a purity range of 99.7 to 99.9%, with major impurities of iron (Fe), silicon (Si), zinc (Zn), and gallium (Ga). While this purity range is sufficient for most industrial applications and alloying, the use of aluminum in high-technology fields, such as semiconductor, electronics, superconducting, and so forth requires higher purity levels exceeding the ones obtained via classical aluminum production processes [1,2]. To reach such purity, several technologies have been developed. There is no officially standardized terminology for the various levels of purity in aluminum. As seen in Table 1, different countries classify the aluminum following their own criteria [3,4].

Due to the extremely low amount of impurities in the base metal, its purity level is described as a function of “Nines”. For example, a base metal, in which the sum of the all targeted impurities is equal to 10 ppm, will have a purity of 99.999%, or 5N (“five Nines”). Moreover, a metal with 5 ppm of impurities would have 99.9995% purity and would therefore be described as 5N5.

Table 1. Classification of various aluminum purity terminologies in USA, China, Russia, and Japan, data from [2,3].

| Country | Designation/Category | Purity (%) | | | Nines | | |
|---------|----------------------|---------------|---|---------|-------|---|-----|
| USA | Commercial purity | 99.50 | - | 99.79 | 2N5 | - | 2N7 |
| | High purity | 99.80 | - | 99.949 | 2N8 | - | 3N4 |
| | Super purity | 99.950 | - | 99.9959 | 3N5 | - | 4N5 |
| | Extreme purity | 99.996 | - | 99.999 | 4N6 | - | 5N |
| | Ultra purity | ≥ 99.999 | | | 5N+ | | |
| China | Primary Al | 99.0 | - | 99.85 | 2N | - | 2N8 |
| | Refined Al | 99.95 | - | 99.996 | 3N5 | - | 4N6 |
| | High purity Al | ≥ 99.996 | | | >4N6 | | |
| Japan | Second grade | 99.950 | - | 99.990 | 3N5 | - | 4N |
| | First grade | 99.990 | - | 99.995 | 4N | - | 4N5 |
| | Special grade | ≥ 99.995 | | | >4N5 | | |
| Russia | Commercial purity | 99.0 | - | 99.85 | 2N | - | 2N8 |
| | High purity | 99.95 | - | 99.995 | 3N5 | - | 4N5 |
| | Ultra purity | ≥ 99.999 | | | 5N+ | | |

2. Main Applications from High-Up to Ultra-High-Purity Aluminum

The aluminum in its high purity has outstanding properties, such as high electric and thermal conductivity. Additionally, when an oxide layer is formed over its surface, high corrosion resistance and electrical insulation can be achieved. Such characteristics grant the usage of high-purity aluminum in integrated circuits, replacing Cu and Au as bonding wires for transistors, where thin films of high-purity aluminum are able to find applications as interconnecting lines in very large-scale integrated (VLSI) circuits [5–7].

Further properties of high-purity aluminum are the low magnetic permeability, the absence of low-temperature brittleness, as well as the increased strength and plasticity at low temperatures [8]. These explain the classical application of high- to ultra-high-purity aluminum for the stabilization of superconductors running at cryogenic temperatures as low as $-269\text{ }^{\circ}\text{C}$ [9].

Due to its beneficial performances, the application of this material in modern high-technology fields grows together with the advances of modern society. The ever-increasing power efficiency and zero-defect tolerances in the high-tech applications will most likely push the technical requirements and purity tolerances of high- and ultra-high-purity aluminum. The subsections below illustrate some classical utilizations of high-purity aluminum at specific purity ranges.

2.1. 3N8–4N8 Purity

At this purity level, more than 75% of aluminum is used as foils for the production of electrolytic capacitors. This application requires a purity of 99.95% for the anode foil and 99.998% for the cathode foil. The aluminum electrolytic capacitors find its application in a broad range of products and technologies, among which are rail vehicles, studio surge-measuring instruments, fluorescent lights, and video equipment [10]. Moreover, this purity range allows the aluminum to be rolled with a mirror-like surface quality, granting a very high reflective index surface that allows it to be used in reflectors [11,12]. Another use of aluminum at this purity level is as a component of superalloys, which are used for the manufacturing of, for example, rocket thrusters and low-pressure gas turbines. As a single crystal, this type of superalloy shows high strength and oxidation resistance at elevated temperatures, thus improving the working performance and efficiency of the equipment [12].

In the superconductor applications, this material is applied in rectifier wires and stabilizing materials. For instance, some of the superconducting cables from the detector in the European Nuclear Research Center (CERN) is made of high-purity aluminum [13].

2.2. 5N+ Purity

Around 96% of 5N+ pure aluminum is mostly used in semiconductor industries, while 4% is used in superconductor applications. At these purity ranges, the total amount of impurities present is less than 10 ppm [14].

This class of material is required by the manufacturing of optoelectronic storage media, such as CDs, DVDs, and so forth. Furthermore, the aluminum can be processed into the electrical conductor of the computer storage hard disk via the cathode-sputtering process [12].

Ultra-high-purity aluminum can also be used as a sputtered coating during the manufacturing of integrated circuits [15]. In this application, not only is the overall purity of the aluminum critical, but also the specific content of elements, such as thorium and uranium. When over a few ppb, the radioactive nature of such α -emitter elements yields malfunction in the integrated circuit, causing programming errors [16].

Moreover, aluminum at this purity level can also be used for base scientific investigations, such as modeling of the solid-liquid interface, and the theoretical model of the formation and evolution of the crystalline phase structures in the solidification system [17].

3. The Production of High- and Ultra-High-Purity Aluminum

The high-volume and industrial production of high-purity aluminum follow two main routes: three-layer electrolysis and fractional crystallization. While both processes can individually reach 4N8 purity, higher purity levels can be obtained when employing them in series. Alternative routes, such as vacuum distillation and organic electrolysis, are reported in the literature and can be used for low volume production and/or highly specialized applications.

The availability of public information regarding price, production volume, and main consumers are very scarce and quite often regarded as a trade secret among the industry. The small amount of public information available was compiled in the Table 2 [12].

Table 2. The production capacity of high- and ultra-high-purity aluminum in the world in 2003.

| Country | Three-Layer Electrolysis (kt/a) | Segregation (kt/a) | World Total (kt/a) |
|---------------|---------------------------------|--------------------|--------------------|
| Japan | 5.2 | 34.3 | 39.5 |
| Norway | 8.0 | — | 8.0 |
| Russia | 15.0 | — | 15.0 |
| China | 28.0 | 5.0 | 33.0 |
| United States | — | 20.0 | 20.0 |
| Germany | 4.5 | 7.0 | 11.5 |
| France | 2.0 | — | 2.0 |
| World total | 62.7 | 66.3 | 129.0 |

The price of high-purity aluminum increases exponentially according to its purity degree (see Table 3). According to the London Metal Exchange (LME), the price of 2N7 Al was 2.45 \$/kg in June 2021 [18]. Despite the variance between suppliers and the format (ingot, foil, etc.), a price range for several aluminum purities was obtained from the company Laurand Associates Inc, where, for the same period, the price per kilogram of pellets ranges from 275 US\$ for 4N up to 900 US\$ for 6N purity [19].

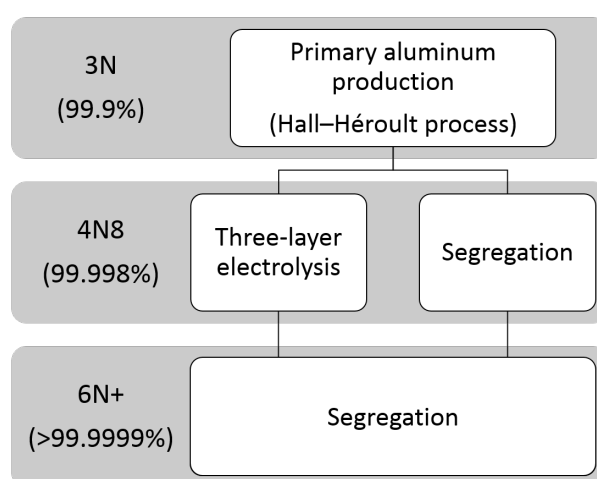
Table 3. The price per kilogram of aluminum in the western market in 2021, data from [18,19].

| Purity | Price (Western Spot Market, \$/kg) |
|--------|------------------------------------|
| 2N7 | 2.45 |
| 4N | 275 |
| 4N6 | 300 |
| 5N | 600 |
| 6N | 900 |

4. Methodologies for the Production of High- and Ultra-High-Purity Aluminum

The technical purity limit achieved in the primary aluminum production (via Hall–Héroult process) ranges from 99.5% up to 99.9% [3]. To achieve an aluminum purity higher than that of primary production, the three-layer electrolysis and the segregation (a.k.a fractional crystallization) processes are the main technologies currently employed. In practice, each of them could be individually performed to produce up to 4N8 aluminum [20,21]. An overview of the processing routes can be seen in Figure 1 [22].

Since three-layer electrolysis cannot achieve purity levels higher than 4N8–5N, the production of higher purities (5N+) requires either the combination of both methods (three-layer electrolysis followed by segregation) or relies solely on segregation by means of several process repetitions [22]. Other technologies, such as vacuum distillation and organic electrolysis, can also be employed to achieve higher purities of aluminum.

**Figure 1.** The process of high- and ultra-high-purity aluminum production.

4.1. Three-Layer Electrolysis

The method of three-layer electrolysis was firstly introduced in 1901 by Hoopes of the Alcoa Research Laboratories [23]. Since then, this method has been improved over the years in order to increase the purity and costs of the output aluminum [23,24].

The structure of a modern three-layer electrolytic cell is shown in Figure 2. The outer layer of the equipment is made of steel, and the bottom is composed of an anode carbon block, as well as refractory brick for heat preservation. The side wall in contact with the melt is built with refractory magnesia bricks. Over the top, a cathode made of graphite is connected [24].

The process works by dissolving commercial-grade aluminum (99.7%) in copper, forming an Al–Cu ($33 \pm 3\%$ Cu) master alloy, which is used as a high-density ($3.4\sim 3.7\text{ g}\cdot\text{cm}^{-3}$) anode at the bottom of the cell. The middle layer is composed of an electrolyte ($2.7\sim 2.8\text{ g}\cdot\text{cm}^{-3}$), and the upper layer, where the extracted high-purity aluminum ($2.3\text{ g}\cdot\text{cm}^{-3}$) is located. The density differences of each layer, as well as the presence of an electrolyte layer in the middle portion of the melt, ensure that both the Al–Cu and the formed high-purity aluminum layers are stable and separated during the electrolysis process [25].

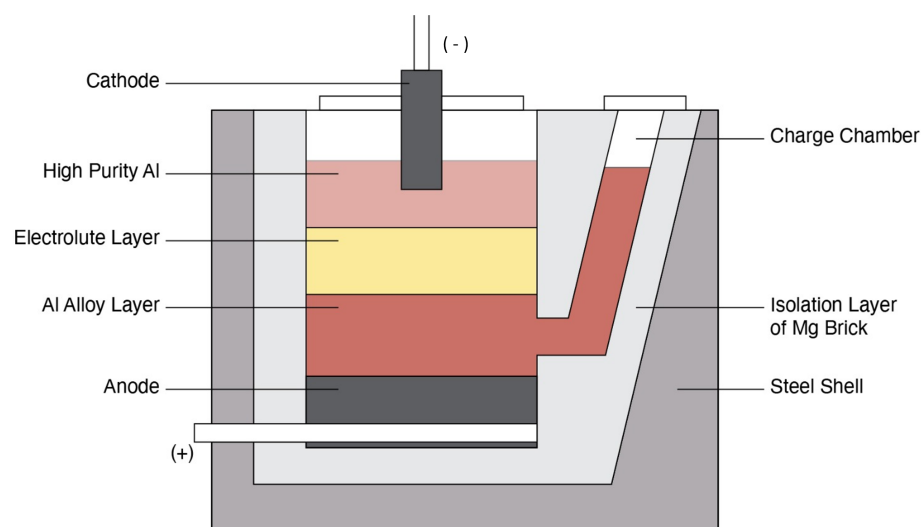


Figure 2. Structural sketch of three-layer electrolytic cell, data from [24].

As the high-purity aluminum migrates through the electrolyte towards the upper layer, more aluminum needs to be added to the Al-Cu alloy. In this process, copper is used to improve the density and to lower the melting point to $\sim 548\text{ }^{\circ}\text{C}$ (for an eutectic composition of 33% Cu). After several cycles of electrolysis, the impurities present in the commercial-grade aluminum remains concentrated in the anode. In the specific case of Fe, its concentration increase in the anode raises the melting point of the master alloy, making the electrolysis process less efficient. Therefore, the master alloy needs to be replaced every 2~3 years [24].

The electrolytes currently used are usually composed of fluoride or chloride, such as sodium, barium, aluminum, calcium, and magnesium. Although the composition varies between companies, they nevertheless have to meet the following requirements:

- Density located between the upper high-purity Al layer and the Al-Cu anode master alloy;
- Chemical stability and low volatility at the electrolysis temperature;
- Low electric resistance;
- Slightly higher melting point than high-purity Al;
- Contained metallic elements and with higher activity than aluminum;
- Weak reaction with the electrolytic cell refractory.

The main components of the electrolyte, as well as its main effects on the process can be seen in Table 4. It can be seen that barium compounds are indispensable because of their high density. Further elements are added to control aspects, such as melting point and conductivity.

Table 4. The role of each component of the electrolyte, data from [24].

| Component | Effect on Electrolyte |
|--------------------------------------|--|
| BaCl ₂ , BaF ₂ | Increases density |
| NaF | Increases conductivity |
| AlF ₃ | Lowers the melting point and increases Al ions |
| CaF ₂ | Lowers the melting point |
| MgF ₂ | Lowers the melting point |

The purification principle of the three-layer electrolysis is to use the electrode potential differences of metal ions in the electrolyte. That means that the elements more positively charged than Al, such as Fe, Si, Cu, and Mn, will remain in the master alloy, while the more

negatively charged elements, such as Na, Ca, Ba, and Mg, will be ionized together with Al; however, Al^{3+} ions are preferentially precipitated at the cathode, and the others will stay in the electrolyte and be eventually deposited in the refractory walls.

The thickness of the master alloy layer is around 200~300 mm, while the electrolyte layer and high-purity Al layer are around 100~200 mm and 100~150 mm, respectively. The DC power consumption is usually 13,000 kWh/t aluminum, and the current efficiency is 95~98% [24]. It is reported in the literature that a productivity rate of up to 20,000 t/year can be obtained by a series of 85 KA cells [2]. The purity of aluminum obtained by this method can finally achieve up to 4N8, with the main residual impurities being a few ppms of Fe, Si, Zn, Mg, and Cu [25].

Reported End-Purification

This method has been reported to achieve between 4N8 and 5N, starting from metallurgical-grade aluminum (2N8). This represents an overall impurity reduction factor of up to 99.5%. Due to its scalability and process simplicity, the three-layer electrolysis is among the few cost-effective techniques for removing impurities from the aluminum up to 5N range.

4.2. Vacuum Distillation

In terms of theoretical analysis, the saturated vapor pressure and the separation coefficient β are two main criteria for predicting the separation effect of impurities by vacuum distillation. For the first criterion, elements with more highly saturated vapor pressure can be more easily volatilized into the gas state under certain conditions; thus, the separation can be realized when some elements escape from the liquid melt and then condensed on the cooling area. The relationship between the saturated vapor pressure and temperature can be derived as shown in Equation (1) [26].

$$\log p^* = A \cdot T^{-1} + B \cdot \log T + C \cdot T + D, \quad (1)$$

where p^* is the saturated vapor pressure, Pa; T is the temperature, K; and A, B, C, D are the evaporation constants. The evaporation constants of the main impurities in primary aluminum are listed in Table 5.

Table 5. The saturation vapor pressure constants of some elements at given temperatures, data from [26].

| Elements | A | B | C | D | T/K |
|----------|---------|--------|---|--------|-----------|
| Al | 6380 | −1.0 | / | 14.445 | 933~2793 |
| Cu | −17,770 | −0.86 | / | 14.42 | 298~1358 |
| | −17,520 | −1.21 | / | 15.335 | 1358~2836 |
| Fe | −21,080 | −2.14 | / | 19.02 | 298~1811 |
| | −19,710 | −1.27 | / | 15.395 | 1811~3135 |
| Mg | −7780 | −0.855 | / | 13.54 | 298~923 |
| | −7550 | −1.41 | / | 14.915 | 923~1363 |
| Mn | −14,520 | −3.02 | / | 21.365 | 1519~2335 |
| Ni | −22,500 | −0.96 | / | 15.72 | 298~1728 |
| | −22,400 | −2.01 | / | 19.075 | 1728~3187 |
| Pb | −10,130 | −0.985 | / | 13.285 | 600~2023 |
| Si | −23,550 | −0.565 | / | 14.48 | 298~1687 |
| | −20,900 | −0.565 | / | 12.905 | 1687~3540 |
| Ti | −23,200 | −0.66 | / | 13.865 | 1943~3562 |
| Zn | −6850 | −0.755 | / | 13.36 | 298~693 |
| | −6620 | −1.255 | / | 14.465 | 693~1180 |

According to Equation (1) and Table 5, the relationship between the saturated vapor pressure and temperature of those elements can be plotted in Figure 3. It can be seen that the vapor pressures of Zn, Mg, Pb, and Mn are higher than that of Al in the given temperature range, which can be preferentially volatilized during the distillation process. In contrast, elements with lower vapor pressure, such as Fe, Ni, and Si, are kept in the molten part. On the other hand, the impurities with closer vapor pressure to Al, such as copper, are difficult to be removed by vacuum distillation.

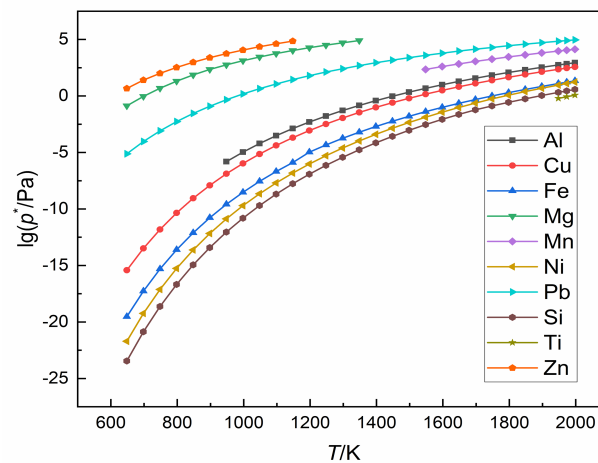


Figure 3. The relationship between the vapor pressure logarithm and the temperature of different elements.

Parallel to the vapor pressure and considering the component activities on separation, a separation coefficient β was introduced to predict the separation effect [26], whose equation can be derived as seen in Equation (2):

$$\beta_i = \frac{\gamma_i \cdot p_i^*}{\gamma_{Al} \cdot p_{Al}^*}, \quad (2)$$

where p_i^* and p_{Al}^* are the saturated vapor pressures of element i and Al at a certain temperature, respectively; and γ_i and γ_{Al} are the activity coefficients of element i and Al at the certain temperature, respectively; and β_i is the separation coefficient of element i . When $\beta_i > 1$, impurity i can be concentrated in the vapor phase, and element Al is maintained in the liquid phase; when $\beta_i < 1$, the situation is correspondingly opposite. Therefore, it means that a better separation effect can be achieved when $\beta_i \gg 1$ or $\beta_i \ll 1$.

For primary aluminum, the composition of all impurities is less than 1%. Considering the system as an infinitely dilute solution, the activity coefficient of γ_{Al} can then be assumed to be in unity, while for the activity coefficient of the impurity, γ_i , it is usually derived from self-calibration of the results of repeated experiments that have been carried out. Specifically, the relationship between the evaporation ratio of a certain impurity element (x_i) and the main metal (x_{Al}) can be expressed as Equation (3) [26].

$$x_i = 1 - (1 - x_{Al})^{\alpha_i}, \quad (3)$$

where α_i is the evaporation coefficient, which can be calculated from the experimental results. The experimental volatilisation ratio can be calculated from the mass loss. Then, the experimental value of the segregation coefficient can be obtained from Equation (4):

$$\beta_i = \alpha_i \cdot \sqrt{M_i / M_{Al}}, \quad (4)$$

where M_i and M_{Al} are the molecular mass of the impurity i and the main metal Al, respectively. After that, the activity coefficient of element i (γ_i) can be concluded by combining Equations (2) and (4).

In addition, these two criteria mentioned above are both used to predict the efficiency of vacuum distillation separation. If a more precise quantitative analysis of the separation is required, the molecular interaction volume model (MIVM) [27,28] will be introduced to estimate the activities of the binary or ternary systems composed of each impurity and the main metal. Then, we plotted the vapor-liquid equilibrium (VLE) diagram for further analysis. Due to the complicated calculation processes and the lack of the MIVM program, VLE diagrams are not discussed in this paper.

Reported End-Purification

No disclosed information regarding the end-purification of aluminum via vacuum distillation was found. The main impurities present in metallurgical-grade aluminum (2N7) consists of Fe and Si. Based on the vapor pressure curves shown in Figure 3, the distillation of aluminum can be theoretically performed by a two-stage distillation process. The first stage would remove the volatile impurities from aluminum (Zn, Mg, Mn, Pb), while the second stage will distill the aluminum itself from the residue impurities.

4.3. Organic Electrolysis

Since the usual process of aqueous electrolysis is not possible to be performed in aluminum due to hydrogen evolution and the strong oxygen affinity of aluminum, the solution found for the electrolysis was to use organic solvents and ionic melts. This method has been developed and successfully applied for the electrodeposition of high-purity aluminum at low temperatures [29,30].

One of the first studies conducted in the 1950s by Hurley et al. already described the potential of this method to obtain a high-purity aluminum layer over a substrate. While the usage of organic electrolysis for the refining of aluminum was explored industrially at the time [31], this method has found a special application as the coating of high-purity aluminum [32] due to its high corrosion resistance. Figure 4 illustrates a deposited aluminum layer over a steel strip by the ionic liquid electrolysis using a bath composed of 60 mol% of AlCl_3 and 40 mol% of [EMIm]Cl (1-Ethyl-3-methylimidazolium chloride) [33].

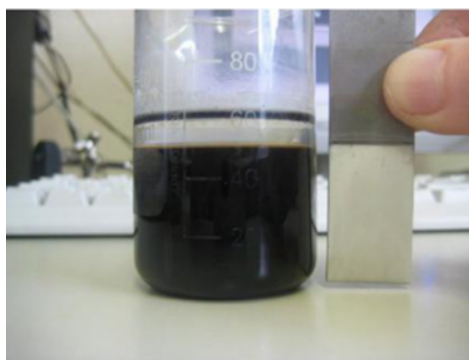


Figure 4. Aluminum deposited over a steel strip by the use of ionic liquid solution organic electrolysis, data from [33].

Past research on this method was mostly focused on the development of electrolyte solutions [29]. Etheric solvents, such as THF (tetrahydrofuran), has been reported as being used industrially by the Japanese company Nissan Steel Co. for the continuous aluminum coating of steel wires and strips, mostly for use in integrated circuits [34]. The company Philips Research also reported achieving 4N purity while using THF solvents for its electroplating process carried out at ambient temperature, with close to 100% current efficiency [34].

Nowadays, the solutions of complexes of Organoaluminum compounds are the most technologically accepted electrolyte systems for aluminum electrodeposition. The “Signal Process” (Siemens Galvano Aluminum Process), first mentioned by Ziegler and Lehmkuhl,

is currently exploited for special corrosion protection of automobile parts. Moreover, the same type of electrolyte has been used for many years, achieving up to 6N purity [34,35].

Besides the coating applications of this method, its use for metal refining was successfully employed industrially [35,36]. According to the 1974 research report from the company VAW (nowadays Hydro High Purity GmbH), its former industrial organic electrolysis cell was able to purify ca. 2 tons per year, obtaining aluminum with 5N5 purity from a 4N initial material, whose equipment and the obtained product are illustrated in Figure 5 [36].

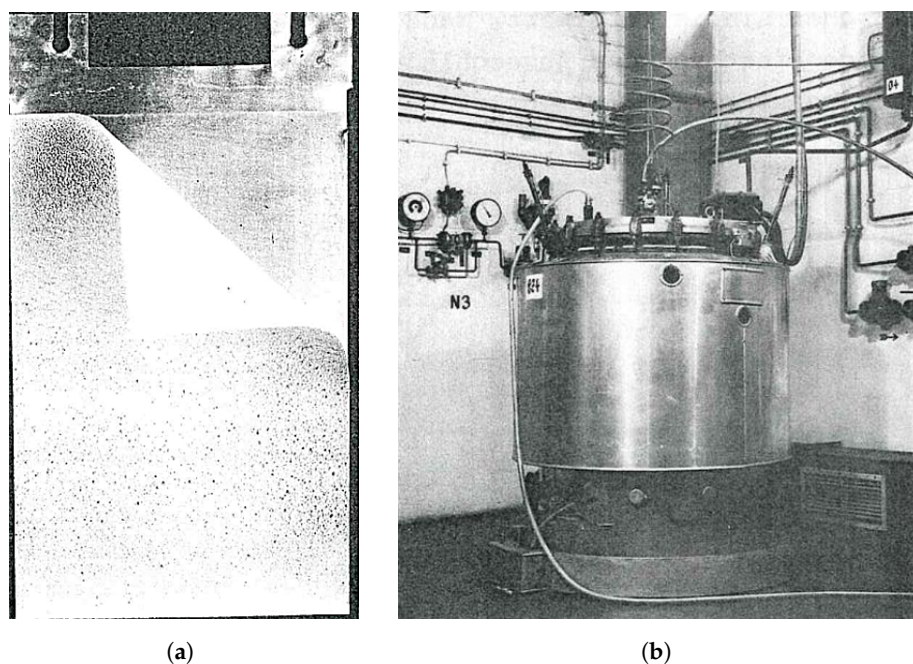


Figure 5. (a) High-purity refined aluminum deposited over cathode and (b) industrial-scale organic electrolysis cells at VAW.

Within the scope of aluminum refining, Wu et al. investigated the use of ionic liquids for refining aluminum at low temperatures (105 °C), where the impurer aluminum was dissolved at the anode and >99.9% pure aluminum was deposited over a copper cathode. Despite the relatively low purification level achieved, the required energy consumption was reported to be only about 3 kWh/kg at a cell voltage of 1V and a current density between 310 and 730 A/cm² [29,37,38]. With further developments, this process can be a promising alternative to the energy-intensive three-layer electrolysis.

Reported End-Purification

The yearly refining of ca. 2 ton of 4N aluminum into 5N5 purity via organic electrolysis has been reported by the former company VAW. Moreover, up to 6N purity aluminum coating was achieved by the signaling process.

4.4. Segregation

The general term of segregation denotes a family of methods that takes advantage of the difference between the solubility of impurities in liquid and solid phases of a base metal. A key indicator of the difference in solubility is the distribution coefficient “*k*” (Equation (5)), calculated as the ratio between the concentration of a specific impurity in both solid (*C_S*) and liquid (*C_L*) phases. Both impurity concentrations can be easily obtained from a binary phase diagram through the lever rule [39,40].

$$k = \frac{C_S}{C_L} \quad (5)$$

The impurities that have a $k > 1$ will tend to be incorporated by the base metal upon crystallization, while for the impurities, their $k < 1$ will be segregated towards the liquid phase. In the rare cases where the impurities have $k = 1$, there will be no segregation and the impurity will be equally dispersed in the matrix. In general, the further the impurity is from unity, the easier it is for them to be segregated upon crystallization. The Table 6 illustrates the distribution coefficient for the main impurities in aluminum [41].

Table 6. The distribution coefficient (k) of main impurities in aluminum.

| Element | Range of k | Element | Range of k |
|---------|--------------|---------|--------------|
| Pb | 0.0007 | Ag | 0.2–0.3 |
| Ni | 0.004–0.09 | Mg | 0.29–0.5 |
| Ca | 0.006–0.08 | Zn | 0.35–0.47 |
| P | <0.01 | Mn | 0.55–0.9 |
| Na | 0.013 | K | 0.56 |
| Fe | 0.018–0.053 | Sc | 0.9 |
| Si | 0.082–0.12 | Cr | 1.8 |
| Sb | 0.09 | Zr | 2.3–3 |
| Cu | 0.15–0.153 | V | 3.3–3.4 |
| Au | 0.18 | Ti | 7–11 |

In spite of this coefficient being a good indicator of the expected impurity segregation during fractional crystallization, a more realistic approach can be evaluated by taking the growth rate of the solid, the diffusion of the impurity into the melt, and the thickness of the diffusion boundary layer into account. This optimized approach leads to the so-called effective distribution coefficient (k_{eff}), shown in Equation (6) and first introduced by Burton, Prim, and Slichter (known as the BPS model) [42].

$$k_{eff} = \frac{k}{k + (1 - k) \cdot e^{[-V\delta/D]}}, \quad (6)$$

where k is the distribution coefficient, V the solid growth rate, δ is the thickness of the diffusion layer, and D is the solute diffusion coefficient in the liquid.

4.4.1. Layer- and Suspension-Based Segregation Method

Several methods have been developed over the years to achieve the purification of aluminum via segregation. In spite of the differences between the methodologies, one can separate them into two main categories: Layer-based segregation and suspension-based segregation. When, during the crystallization, the formed crystals grow attached to a surface, forming a layer, the method is denominated as “layer-based”. If the crystals grow freely suspended in the melt, it is called “suspension-based” [43]. A schematic representation of both categories of the segregation process can be seen in Figure 6.

The suspension-based method has the advantage of a higher solid/liquid interface area, where the impurities can be segregated out of each individual crystal formed (see Figure 6, left). The resulting crystal, which has a higher purity and slightly higher melting point than the adjacent melt, settles down to the bottom of the furnace. Contrarily to the above-mentioned method, layer-based segregation has the advantage of no additional method to separate the formed crystals from the bulk melt, as the crystallization occurs over the previously crystallized portion (see dotted line from Figure 6, right), that is, the solid phase grows continuously. This ultimately not only facilitates the process, but avoids the entrapment of an impurity-rich melt within the purified product. To minimize this effect, some of the suspension-based techniques takes advantage of a tampering system to compress the crystals and expel the melt within the settled material.

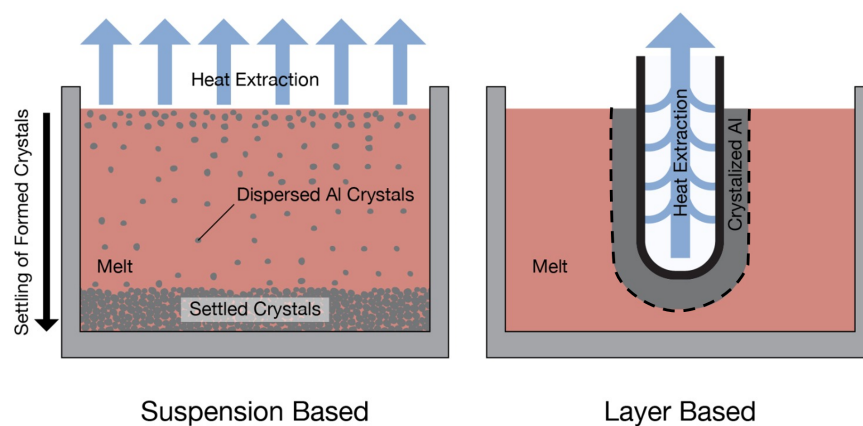


Figure 6. Sketch representation of suspension-based (left) and layer-based (right) segregation methods.

4.4.2. Suspension-Based Segregation Techniques

Alcoa Process

The company Alcoa (nowadays Arconic Inc., Pittsburgh, PA, USA) developed in the late 1960s was a suspension-based segregation method for the production of high-purity aluminum. The output aluminum reached up to 6N purity in a two-stage crystallization process [44].

While being employed as a subsequent step after the three-layer electrolysis, it can also be used as a single step, where metallurgical-grade aluminum (2N8) is purified to 4N purity with lower costs compared to the electrolysis route [45]. The Figure 7 shows a sketch of this technique [44].

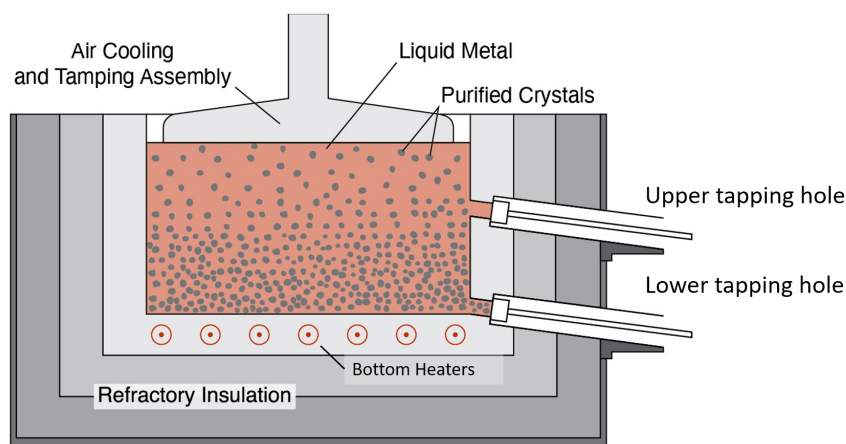


Figure 7. Sketch representation of the Alcoa segregation technique, data from [44].

The process works by slowly cooling the surface of the molten aluminum bath, creating purified aluminum crystals that will settle to the furnace bottom due to its higher density. The remaining liquid contains the segregated impurities from the formed crystals. To prevent crust formation on the melt surface and compact the settled crystals, a mechanic tamper is used [46]. A different version of this process employs a series of burners over the melt to prevent the formation of crusts on the melt surface, and also uses small tampers to compact the crystals [45].

As with any other segregation method, the precise control of temperature is extremely important. To avoid the total freeze of the interstitial molten aluminum between the formed crystals, the temperature is carefully controlled by a series of heaters at the furnace bottom. The pressing process, promoted by the mechanical tamper, will then be able to expel the liquid interstitial aluminum (containing most of segregated impurities), leaving a layer of

purified aluminum crystals. At the end, the charge consists of a semisolid mass of purified aluminum crystals and a top layer of molten aluminum containing most of the segregated impurities [15,46,47].

To extract the purified aluminum, firstly, the molten top aluminum layer is poured via an upper tap hole. Later, the purified semisolid layer of aluminum is melted again by the increase of the temperature in the bottom heaters, and tapped via a lower tap hole [15,47].

Reported End-Purification

The Table 7 below summarized a typical purity obtained in this process, as well as the impurities content present in each purity level [47].

Table 7. Typical obtained aluminum purity grade and its impurity content—in ppm, data from [47].

| Al | Si | Fe | Cu | Mn | Mg | Cr | Ni | Zn | Ti | V | B | Ga | Zr |
|-----|-----|-----|-----|-----|-----|-----|-------|------|------|------|-----|-------|------|
| 3N6 | 135 | 165 | 10 | 13 | 4 | 2 | 10 | 10 | 10 | 10 | 6 | 70 | 10 |
| 3N8 | 69 | 60 | 3 | 9 | 4 | 2 | 3 | 5 | 6 | 13 | 4 | 42 | 10 |
| 4N3 | 22 | 18 | 2 | 5 | 1 | 1 | 0 | 5 | 0 | 2 | 2 | 11 | 3 |
| 4N7 | 7 | 4 | 3 | 0 | 1 | 1 | 0 | 1 | 1 | 1 | 1 | 2 | 1 |
| 5N5 | 0.7 | 0.2 | 0.3 | 0.1 | 0.5 | 0.1 | 0.005 | 0.05 | 0.05 | 0.01 | 0.1 | 0.005 | 0.01 |

Corus Crystallizer

This technique was originally developed by the former Dutch company Corus Technology BV, and functions as a continuous suspension-based process (see Figure 8) [48]. This technique works by inserting the molten aluminum in the crystallizer chamber. The molten aluminum (represented as both a red and yellow color in Figure 8) floats over the cooling liquid, as it has a lower density than the cooling liquid composed of a mixture of molten salts (orange color). A series of cooling units (in blue color) cools the cooling liquid, which also has the function of slowly extracting heat from the molten aluminum layer. This will then induce the formation of pure aluminum crystals in the aluminum melt [43].

The molten salt mixture is pumped and circulates via a pipe from one extremity of the crystallizer to another. Moreover, it is also slowly cooled by a heat exchange unit. The flow of molten salt, together with the convection generated by the temperature gradient in the molten aluminum, transports the pure aluminum crystals towards the exit (right upper side of Figure 8), while the residual melt flows towards the exit (left upper side of Figure 8). Furthermore, a series of wall baffles and impellers are installed inside the chamber with the aim of avoiding the mixing of purer and impurer aluminum melt, in a way that the chambers located on the left contains more impurities than the ones on the right [48].

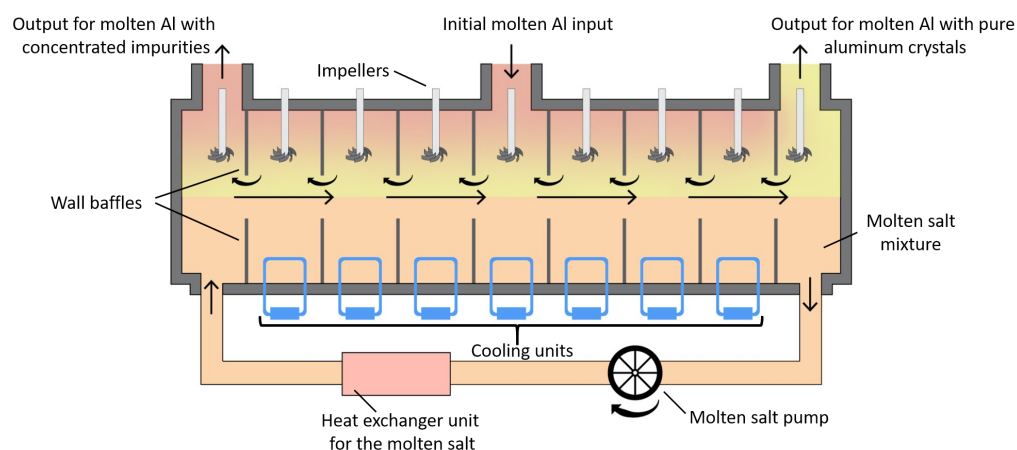


Figure 8. Sketch of the corus crystallizer technique—adapted from [48].

This technique is reported to be able to process up to 20 tons per day, elevating the purity of a P1020-grade aluminum (0.1% Si and 0.2% Fe) into a P0101-grade aluminum (0.01% Si and 0.01% Fe) [48].

From the little information available, it is assumed that the most critical parameter is the control of the molten salt temperature, as it directly controls the crystallization rate (and therefore, impurity segregation) in the melt. Moreover, the temperature gradient induced in the process is responsible for the flow of purified metal towards the chamber exit [43,48].

Additionally, the positioning and speed of the impellers and wall baffles can be controlled in order to improve the yield of the purified aluminum fraction [43,48].

Reported End-Purification

Despite being originally developed for the upgrade of recycled aluminum into a product with purity closer to primary aluminum (2N8) [48], its characteristics allows it to be used for the production of high-purity aluminum when fed with cleaner aluminum, or when consecutive process cycles are run [43].

4.4.3. Layer-Based Segregation Techniques

Zone Refining

Figure 9 shows the schematic diagram of zone-refining. This technology is an effective method to perform further purification of the purchased raw materials, which do not currently meet the requirements of high-purity metals for advanced technologies [49]. A molten zone passes through the charge in one direction, exhibiting a difference in impurity concentration between the liquid and the freezing solid. If the impurity concentration in the freezing solid higher than in the liquid, this impurity will be concentrated in the first portion during the ingot solidification. On the contrary, the concentration in freezing solids will be lower than in the liquid. Hence, the impurity will be rejected by the freezing solid and travel with the zones and accumulate at the end of the charge, thereby purifying the remainder. Zone-refining is more advantageous in purifying the purer starting materials. The dominant factors influenced the purity level of the high-purity aluminum ingots, including zone length, zone passes, freezing interface moving speed, and temperature gradient.

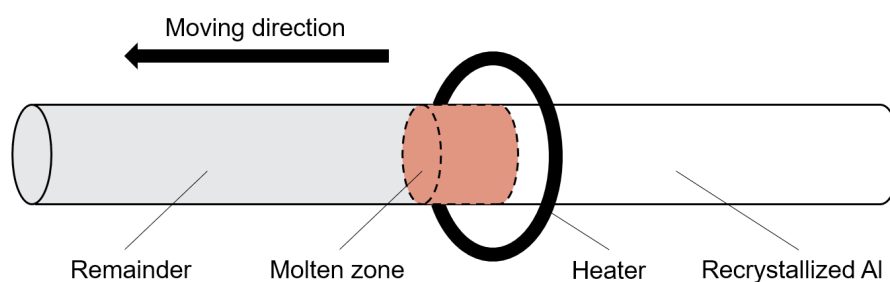


Figure 9. Structural representation of the zone-refining process with a single heater.

Zone Length (z)

It is clear that the zone length appears in nearly all quantitative expressions concerning redistribution of solutes during the process [50,51]. Some attempts have been made to improve the refining efficiency by considering the effect of zone length on solute redistribution [52,53].

The separations obtained in the process with adjustable zone length are much better than those in the process with constant zone length for all values of the equilibrium distribution coefficient, k , which is a concentration ratio (C_S/C_L) of solute in the freezing solid to that in the liquid. The maximum separation with the first pass is achieved when the zone length z , is equal to L , the length of the ingot; that is, the best performance in the first pass is achieved by a normal-freezing operation [54,55]. To fulfill the optimization condition, it is necessary to minimize the total solute content of any such volume of freezing

material, over any time increment by controlling the movement of the melting interface. It has been proved that the optimum condition occurs when the composition of the molten zone equals that of the solid about to be melted [56].

Zone Passes (n)

The efficiency of zone refining is strongly influenced by the number of zone passes [57]. Fewer passes cannot attain the product with high purity, while more passes consume more time. Moreover, it is reported that 20-time passing decreases the resistance ratio when compared with 10-time passing [58]. It means that the purification efficiency saturates at a level when an amount of passing is reached, and further zone-passing rather contaminates the ingot.

In general, the ultimate distribution, which is a function of zone length, is steadily reached in the case of shorter zone length [56]. It can be concluded that the zone-refining technique will not result in appreciable purification, even by repeated pass methods for cases where the zone travel rate and zone length are relatively large [59]. Some results have validated this claim, that the concentration distribution profile would be stable with longer zone length approaches in 10 passes [57,60].

Solid/Liquid Interface Moving Rate (f)

According to the work from Burton, Prim, and Schlichter (Equation (6)), we can conclude that low zone movement velocity and intensive convection in the melt could result in a lower k_{eff} if $k < 1$, and a higher k_{eff} if $k > 1$ [42].

Moreover, higher travel rates makes for a short time to permit more passes of the molten zone per unit of time. However, large f is limited by the constitutional supercooling, which is directly related to entrapment of solutes by sudden fluctuations in the shape of the S/L interface. Large f can cause the temperature as maintained by the gradient in the liquid to be lower than the liquidus temperature, as predicted by the equilibrium diagram, and then this part of the liquid will be constitutionally supercooled [61]. The moving rate can be expressed by Equation (7) [55].

$$f \leq \frac{G \cdot D \cdot k}{m \cdot C_S \cdot (1 - k)}, \quad (7)$$

where G is the temperature gradient in the liquid and C_S is the solute concentration, both at the freezing interface; m is the slope of the liquidus line, and f is equal to the heater movement velocity.

Higher zone speeds yields better segregation, when the diffusion layer thickness became small, which is possible only when the stirring mechanism is adopted to produce strong convection in the molten zone [57]. Because the solute concentration profiles vary along each zone pass, an ultra-pure material can be obtained by adopting a continuous variation of zone rate according to the evolution of C_S [50].

Temperature (T) and the Temperature Gradient ($\Delta T / \Delta x$)

As a common experimental parameter, the temperature has not been studied much because it does not directly appear in the expression of the effective distribution coefficient (Equation (6)). The effect of temperature variation on the mechanism of diffusion of impurities during zone-melting can be expressed theoretically as Equation (8) [62].

$$D_{eff} = \frac{\nu \cdot \sigma \cdot T}{A + B_0 \cdot T}, \quad (8)$$

where D_{eff} is the impurity diffusion coefficient, ν is the velocity of the liquid–solid interface, σ is the thickness of the boundary layer, and the constants A and B are graphically determined for each impurity: $A < 0$, $B > 0$, and $A \gg B$. Comparison between experimental and theoretical values of D_{eff} has confirmed the validity of this new expression. However, buoyancy-driven convective effects related to the radial and axial thermal gradient can

increase the variations of D_{eff} . It means that temperatures of the molten zone which are too high are not convenient to reach an optimal purification. On the other hand, when induction heating is used as a heat source, the temperature increase is often accompanied by an increase of the zone length. In the process of optimizing the zone length, the temperature can automatically be kept slightly higher than the melting point of the ingot [62,63], which is one of the reasons why the temperature is rarely investigated specifically in subsequent studies.

Since a temperature gradient exists at the charge, diffusion of solutes through the interface continues when the molten zone travels through the solid. A high temperature gradient permits traversal of a charge at the high rate, while a low temperature gradient causes the low variation in concentration. That is, a smaller range of temperatures in the block makes for a more uniform solute concentration [55]. Therefore, with this particular scheme, a compromise between uniformity and speed may be necessary. Since the way in which the temperature gradient is impressed on the zone can appreciably affect the travel rate, for zone refining, representative travel rates may be a few millimeters per hour in a temperature gradient of the order of 50 °C/cm [55]. However, this claim has not been verified in subsequent research.

Moreover, other factors, such as fluctuation of the molten zone [64,65], cropping technique [60], matter transport [49], and electric current for impurity transport [66] can also influence the optimization of the zone-refining process.

Reported End-Purification

It is very impressive that after a combination of the three-layer electrolytic refining process and the segregation process, 7N-purity aluminum has been obtained by zone-refining as the final process. The highest residual resistance ratio $R(300\text{ K})/R(4.2\text{ K})$ obtained was about 90,000 in the bulk value, corresponding to 99.99999% aluminum [67].

Pechiney

Once the world's pioneer in the production of high-purity aluminum, the former French company Pechiney Aluminum, provided a valuable contribution to this field by developing a fractional crystallization technique that yields a low-cost and high-quality purified aluminum. The success of this technique encouraged other companies, such as the Japanese company Kyushu Mitsui Aluminum Co, to adopt this technique in its manufacturing process [68]. The Figure 10 shows a schematic representation of this process.

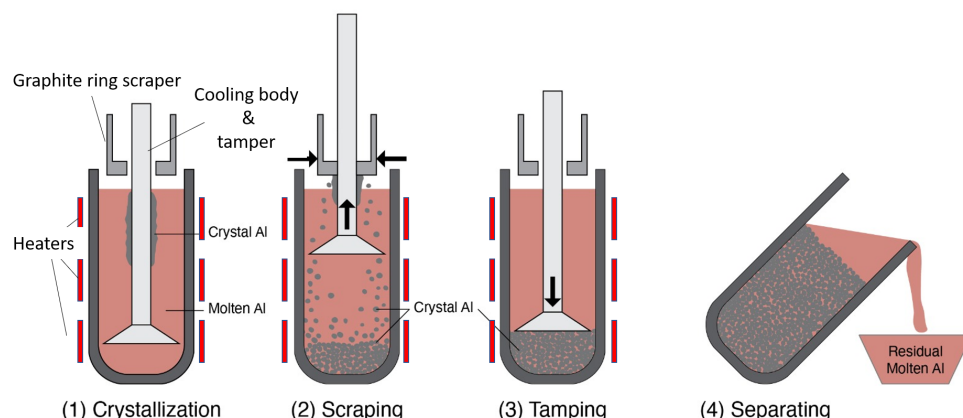


Figure 10. Fractional crystallization sketch of the Pechiney process, as used by Japanese company Kyushu Mitsui Aluminum Co adapted from [68].

Despite being characterized as a layer-based method, this technique also presents a tamping step commonly seen in suspension-based methods. This technique works by firstly melting or pouring molten Aluminum in a resistance-heated crucible, comprised of

several individually controlled heaters. Subsequently, the aluminum is slowly cooled by the immersion of a submerged cooling body. At this stage, the high-purity aluminum is crystallized over the cooling body, and the impurities are segregated to the molten bath.

When the thickness of the crystallized layer is large enough, a graphite ring scraps this layer from the surface of the cooling body. Due to density differences, it settles at the bottom of the crucible and a tamper, installed at the bottom of the cooling body, compresses the formed high-purity aluminum crystals at the crucible bottom, expelling most of the residual melt. The result is a compressed solid layer of high-purity aluminum [68–70].

This process is repeated many times until a thick layer of high-purity aluminum is formed in the crucible bottom. Afterwards, the temperature of the bottom heating elements is slightly increased, and the previously solidified aluminum crystals are partially remelted. This stage of the process is critical to ensure that any residual melt previously entrapped between the crystal layer is remelted and expelled by the tampering process [68,70].

When the desired production yield is achieved (typically 40–70%), the crucible can either be tilted and the residual molten aluminum is poured, or the melt can be left until complete solidification. This requires a later process of sawing the impure fraction of the obtained ingot [69].

Despite being successful in yielding high-purity aluminum, this technique is very sensitive to small changes in temperature and operational conditions. It relies on a precise parallel control of many process parameters, which directly affects the end purity and yield.

Although not much technical literature is available, one can assume that the gas flow rate in the cooling body, the melt temperature, and the bottom heater temperature during re-crystallization are the most critical process parameters in this technique. The combination of the melt temperature and the gas flow rate inside the cooling body is directly responsible for the temperature gradient in the melt. This ultimately influences the crystal growth rate and the respective impurity segregation profile. Moreover, the fine control of the bottom heater is crucial for the partial remelting of the entrapped melt within the formed crystals.

Other aspects of this process, such as tampering conditions like pressure, pistons dimensions, as well as the frequency of tampering play a direct role in the process effectiveness and the final product quality too [68].

Reported End-Purification

According to the Patent from [69], the Pechiney process can purify an initial 3N Aluminum up to 4N with a single process step. Further processing would then yield an even higher purity.

Cooled Finger

The cooled finger technique is one of the latest aluminum purification technologies available. Inspired by the patent from the Japanese Showa Aluminum Corporation [71], its simplicity, purification yield, and processing time positions it among the most promising techniques to produce high- and ultra-high-purity aluminum. A sketch of the cooled finger setup can be seen in Figure 11a. More recently, a laboratory scale of the cooled finger has been developed at the IME institute of RWTH Aachen university for the refining of metals, including aluminum. A sketch of this equipment can be seen in Figure 11b.

The cooled finger consists mainly of a double-walled, fluid cooled rotating steel shaft, covered by a ceramic or graphite sleeve. The setup is inserted in a crucible inside an electric furnace, in which the aluminum is molten and maintained at a specific temperature. The graphite-covered shaft is the one in charge of creating the temperature gradient necessary to grow a purified metallic layer around it. After a specified quantity of aluminum has been deposited, the cooled body is withdrawn from the melt, and the purified aluminum is collected [41,72]. The Figure 12 illustrates an example of a crystallized aluminum product via the cooled finger technique [72].

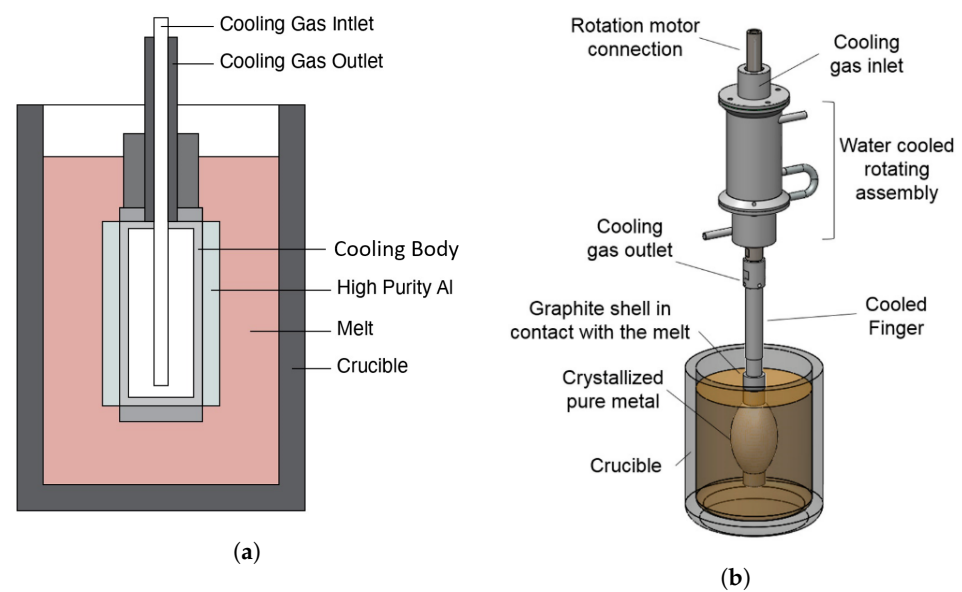


Figure 11. (a) Fractional crystallization sketch of the cooled finger process, as used by Japanese Showa Aluminum Corporation, adapted from [71] and (b) fractional crystallization sketch of the cooled finger process developed at the IME institute from RWTH Aachen University, adapted from [41].

Similar to the Pechiney technique, the cooled finger is subjected to very fine adjustments on the cooling gas flow rate and melt temperature in order to control the crystallization rate. Furthermore, the rotation of the shaft is thought to help in homogenizing the solute concentration in the melt, distributing the rejected solutes faster than natural convection. In other words, by promoting the dilution of the solute located at the growth front towards the bulk liquid by forced convection, it thus reduces the thickness of the diffusion boundary layer ahead of the solidification front. This ultimately leads to a better segregation rate [41].

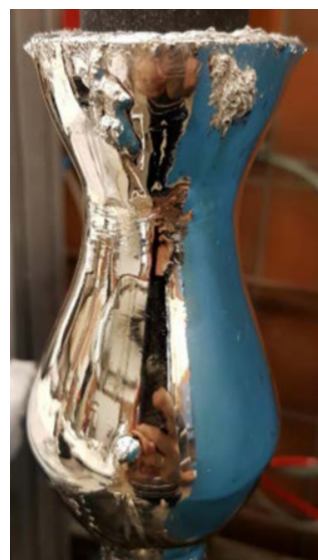


Figure 12. Example of a crystallized aluminum product via the cooled finger technique, adapted from [72].

Reported End-Purification

According to the Patent from Shingu et. al [71], the Cooled Finger process can purify an initial primary Aluminum (2N8) up to 3N8 with a single process step. Further processing would then yield an even higher purity.

Directional Crystallization

As with any segregation process, the directional crystallization (also referred to in the literature as the vertical gradient freeze (VGF) process) relies on the rejection of solutes at the solid–liquid interface to purify the aluminum. It differs from the previous processes mainly by the fact that the whole batch is first molten and then gradually solidified, starting from the bottom to the top. After the sample has been cooled down, it is extracted from the crucible and cropped to obtain a purified portion of the desired metal [60].

This technique works by employing resistance heaters alongside the crucible to create a temperature gradient that drives the crystallization (see Figure 13). In some cases, a seed crystal is placed at both of the crucibles to influence the growth morphology of the crystallized aluminum. Moreover, a flow of cooling gas can be used to cool down the crucible bottom, increasing the temperature gradient at the early stages of crystallization.

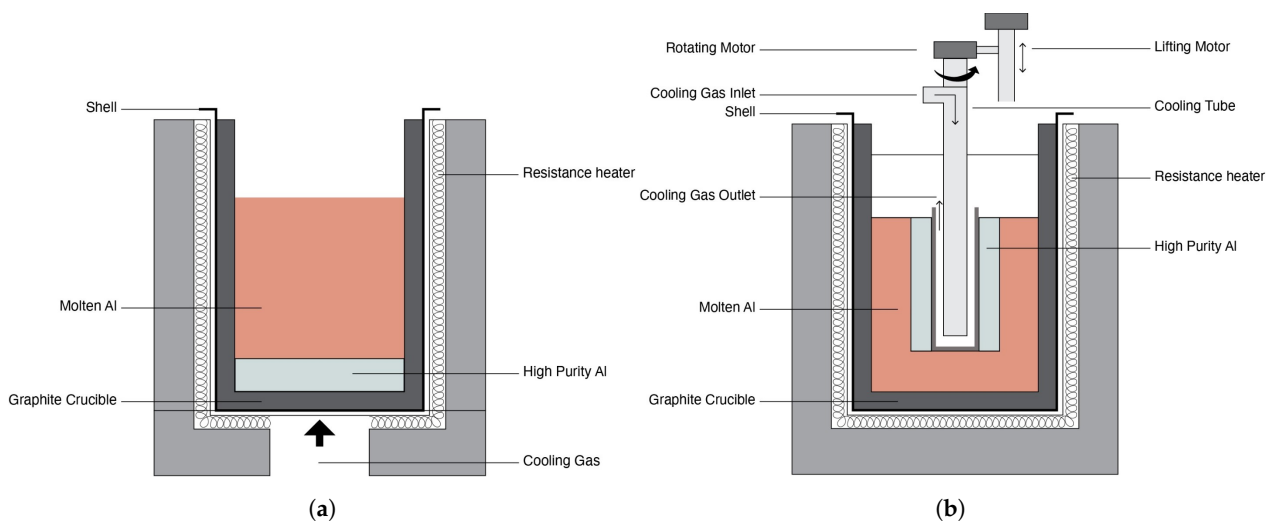


Figure 13. Directional solidification setup (a) without forced mixing and (b) with forced mixing.

As seen in the technique schematics from Figure 13, the process can be employed with and without forced mixing; while without mixing, the growth morphology is better controlled, the additional mixing of the melt assists the removal of the expelled impurities from the growth front, yielding better purification results [24].

The main parameter affecting the impurity segregation is the solid growth rate, which is directly affected by the temperature gradient in the melt. This is mainly induced by the precise combination of heaters temperature profile (by adjusting each individual heater), as well as by the gas flow on the crucible bottom.

In the variation, in which a stirring mixing is applied, the intensity and fluid flow conditions at the solidification boundary also directly affect the impurity segregation profile.

Reported End-Purification

The 5N aluminum was purified by the directional solidification method. The crystal surface temperature was maintained at 660 °C, and the temperature of the molten aluminum surface was maintained at 695 °C to 700 °C. By removing 70% of the thickness of the entire crystalline ingot from the end of the final crystallization ingot, 6N aluminum can be obtained [73].

5. Comparison between Purification Methods

According to the description of the purification methods above, the product purity, and advantages and disadvantages of different technologies are summarized in Table 8. The highest purity can be obtained when zone melting is used as the last procedure to purify high-purity aluminum products. However, from the perspective of achieving low-cost, high-efficiency, and environment-friendly production, the main existing production pro-

cesses still have some defects. Further research on alternative methods or joint innovations may be the key to opening a new era for the industrialization of high-purity aluminum.

Table 8. Comparison of methods for high-purity aluminum production.

| Method | Principle | Technique | Reported End-Purity |
|-------------------|----------------------|----------------------|---------------------|
| Three-layer elec. | Molten salt elec. | - | 4N8–5N |
| Vacuum dist. | Selectively volatil. | - | 5N ^{*1} |
| Organic elec. | Electrolysis | - | 5N5–6N |
| Segregation | Suspension based | Alcoa Process | 5N5 |
| | | Corus Process | 3N ^{*2} |
| | layer-based | Zone melting | 7N |
| | | Pechiney | 4N ^{*3} |
| | | Cooled Finger | 3N8 ^{*3} |
| | | Directional solidif. | 5N–6N ^{*3} |

¹ two-stage distillation. ² Potential for higher values. ³ Single process step.

6. Conclusions

High-purity aluminum has drawn substantial attraction to both scientific and industrial fields during the past few decades. Practically, many efforts have been taken to realize simple and low-cost fabrication procedures, high production efficiency, flexible application, as well as the trade-off among these parameters for HP-Al. Although both vacuum distillation and organic electrolysis achieve high levels of purity, their design and working principles suggest that they would lack the productivity required for high-volume industrial application. Therefore, it can be concluded that the three-layer electrolysis and segregation are still the mainstream industrial production methods. The best product purity that can be obtained by various purification methods and the advantages and disadvantages of different technologies are summarized in this review. This study aims to provide theoretical guide towards the goal of achieving the industrialization of efficient production of high-purity aluminum.

Despite these accomplishments, the eventual industrialization of HP-Al still faces a number of challenges that need to be investigated further. Here is a short list based on our own deliberations:

- Realization of continuous production of kilogram-level 6N+ high-purity aluminum products.
- Improvement of a single process purification method or combined technology.

Author Contributions: Conceptualization, D.C.C., N.X. and S.F.; writing—original draft preparation, D.C.C. and N.X.; writing—review and editing, D.C.C., N.X., S.F., B.F.; supervision, S.F.; principal investigator, B.F. All authors have read and agreed to the published version of the manuscript.

Funding: This research received no external funding.

Institutional Review Board Statement: Not applicable.

Informed Consent Statement: Not applicable.

Data Availability Statement: Not applicable.

Acknowledgments: The authors would like to thank the CNPQ-Brazilian National Council for Scientific and Technological Development for the financial support of the Brazilian scholarship holder D. Curtolo, and the CSC—Chinese Scholarship Council for the financial support of the Chinese scholarship holder N. Xiong.

Conflicts of Interest: The authors declare no conflict of interest.

References

1. Leroy, M. Alpha Rays Emitting Impurities in Ultra Pure Aluminum Evolution Through the Successive Refining Steps. *J. Phys. IV* **1995**, *5*, C7-99–C7-110. [CrossRef]
2. Zhao, H.; Lu, H. The Development of 85kA Three-Layer Electrolysis Cell for Refining of Aluminum. In Proceedings of the TMS Aluminum Committee at the TMS 2008 Annual Meeting & Exhibition, New Orleans, LA, USA, 9–13 March 2008; pp. 533–540.
3. Lindsay, S.J. Very high-purity aluminum: An historical perspective. *JOM* **2014**, *66*, 217–222. [CrossRef]
4. Wang, Z. The properties of high pure aluminum (Part A). *Light Met.* **2004**, *8*, 3–6. (In Chinese) [CrossRef]
5. Head Electronic Co Limited. Guideline for Wire Bonding. Available online: http://www.headpcb.com/html/2018/news&blog_0612/157.html (accessed on 28 June 2021).
6. Sarkar, J.; Saimoto, S.; Mathew, B.; Gilman, P.S. Microstructure, texture and tensile properties of aluminum-2 at.% neodymium alloy as used in flat panel displays. *J. Alloy. Compd.* **2009**, *479*, 719–725. [CrossRef]
7. Onishi, T.; Iwamura, E.; Takagi, K.; Yoshikawa, K. Influence of adding transition metal elements to an aluminum target on electrical resistivity and hillock resistance in sputter-deposited aluminum alloy thin films. *J. Vac. Sci. Technol. A* **1996**, *14*, 2728–2735. [CrossRef]
8. Wang, Z. Talk about the purity aluminum (II). *Met. World* **2004**, *4*, 36–37. (In Chinese) [CrossRef]
9. Zhang, J.; Sun, B.; He, B.; Mao, H.; Chen, G.; Ge, A. Principle and control of new-style purification equipment of 5N high purity aluminum. *Chin. J. Mech. Eng.* **2006**, *42*, 64–68. (In Chinese) [CrossRef]
10. Sankaran, V.A.; Rees, F.L.; Avant, C.S. Electrolytic capacitor life testing and prediction. In Proceedings of the 1997 IEEE Industry Applications Conference Thirty-Second IAS Annual Meeting, New Orleans, LA, USA, 5–9 October 1997; Volume 2, pp. 1058–1065.
11. Chen, Y.; Santos, A.; Ho, D.; Wang, Y.; Kumeria, T.; Li, J.; Wang, C.; Losic, D. On The Generation of Interferometric Colors in High Purity and Technical Grade Aluminum: An Alternative Green Process for Metal Finishing Industry. *Electrochim. Acta* **2015**, *174*, 672–681. [CrossRef]
12. Wang, Z. Production, market and application of high-purity aluminum in the world. *Nonferr. Met. Process.* **2004**, *33*, 1–6. [CrossRef]
13. Miele, P.; ten Kate, H.H. The superconducting magnet system for the ATLAS detector at CERN. *Fusion Eng. Des.* **2001**, *58–59*, 195–203. [CrossRef]
14. Yamagiwa, M.; Yu, Q.; Fujita, M.; Shinohara, M.; Murakami, Y. Reliability study of high-temperature-resistant mounting structure using high-purity aluminum for power devices. *J. Jpn. Inst. Electron. Packag.* **2009**, *12*, 238–247. [CrossRef]
15. Dawless, R.K.; Troup, R.L.; Meier, D.L.; Rohatgi, A. Production of extreme-purity aluminum and silicon by fractional crystallization processing. *J. Cryst. Growth* **1988**, *89*, 68–74. [CrossRef]
16. Al-Medainy, H.S.; Al-Mohawes, N.A.; Chou, H.P. Determination of uranium and thorium concentrations in integrated circuit packaging materials. *J. Radioanal. Nucl. Chem. Lett.* **1989**, *137*, 341–350. [CrossRef]
17. Mahata, A.; Asle Zaeem, M.; Baskes, M.I. Understanding homogeneous nucleation in solidification of aluminum by molecular dynamics simulations. *Model. Simul. Mater. Sci. Eng.* **2018**, *26*, 025007. [CrossRef]
18. The London Metal Exchange. London Metal Exchange Daily Price for Primary Aluminum. Available online: <https://www.lme.com/en-GB/Metals/Non-ferrous/Aluminium/#tabIndex=0> (accessed on 28 June 2021).
19. Laurand Associates Inc. Price of High- and Ultrahigh-Purity Aluminum. Available online: <https://highpurityaluminum.com/products/pellets-slugs-shot?variant=19365073256559> (accessed on 28 June 2021).
20. CAO, P. Comparison and analysis of the preparation methods of high purity aluminum. *World Nonferr. Met.* **2018**, *11*, 10–11. [CrossRef]
21. Gaustad, G.; Olivetti, E.; Kirchain, R. Improving aluminum recycling: A survey of sorting and impurity removal technologies. *Resour. Conserv. Recycl.* **2012**, *58*, 79–87. [CrossRef]
22. Curtolo, D.C.; Rodriguez-Rojas, M.J.; Friedrich, S.; Friedrich, B. Alternative fractional crystallization-based methods to produce high-purity aluminum. *J. Mater. Res. Technol.* **2021**, *12*, 796–806. [CrossRef]
23. Hoopes, W. Process of the purification of aluminium. *arXiv* **1901**, arXiv:1011.1669v3.
24. Wang, Z. Talk about the purity aluminium (III). *Met. World* **2004**, *5*, 33–37. [CrossRef]
25. Kondo, M.; Maeda, H.; Mizuguchi, M. The production of high-purity aluminum in Japan. *JOM* **1990**, *42*, 36–37. [CrossRef]
26. Kong, X.; Yang, B.; Xiong, H.; Liu, D.; Xu, B. Removal of impurities from crude lead with high impurities by vacuum distillation and its analysis. *Vacuum* **2014**, *105*, 17–20. [CrossRef]
27. Tao, D.P. A new model of thermodynamics of liquid mixtures and its application to liquid alloys. *Thermochim. Acta* **2000**, *363*, 105–113. [CrossRef]
28. Tao, D.P. Prediction of activities of all components in the lead-free solder systems Bi-In-Sn and Bi-In-Sn-Zn. *J. Alloy. Compd.* **2008**, *457*, 124–130. [CrossRef]
29. Zhang, M.; Kamavaram, V.; Reddy, R.G. New Electrolytes for Aluminum Production: Ionic Liquids. *JOM* **2003**, *55*, 54–57. [CrossRef]
30. Suneesh, P.V.; Satheesh Babu, T.G.; Ramachandran, T. Electrodeposition of aluminium and aluminium-copper alloys from a room temperature ionic liquid electrolyte containing aluminium chloride and triethylamine hydrochloride. *Int. J. Miner. Metall. Mater.* **2013**, *20*, 909–916. [CrossRef]
31. Gamrath, H.R.; Company, M.C. Process for the Electrolytic Deposition of Aluminum. U.S. Patent 2,849,349, 26 August 1958.

32. Zheng, Y.; Peng, C.; Zheng, Y.; Tian, D.; Zuo, Y. Low-temperature electrolysis of aluminium from 1-butyl-3-methylimidazolium chloroaluminate ionic liquids with inert anode. *Int. J. Electrochem. Sci.* **2016**, *11*, 6095–6109. [\[CrossRef\]](#)
33. Bakkar, A.; Neubert, V. A new method for practical electrodeposition of aluminium from ionic liquids. *Electrochem. Commun.* **2015**, *51*, 113–116. [\[CrossRef\]](#)
34. Zhao, Y.; VanderNoot, T.J. Review: Electrodeposition of aluminium from nonaqueous organic electrolytic systems and room temperature molten salts. *Electrochim. Acta* **1997**, *42*, 3–13. [\[CrossRef\]](#)
35. Böttcher, R.; Ispas, A.; Bund, A. Corrosion Behavior of Aluminum Alloys Deposited from Ionic Liquids. *ECS Meet. Abstr.* **2018**, MA2018-02, 634.
36. Hannibal, W.; Ibe, G.; Kurre, K.; Peychal-Heiling, H.; Pfundt, H.; Reuter, W.; Scharf, G.; Winkhaus, G. *Entwicklung eines technischen Verfahrens zur Herstellung von Reinstaluminium für die Kryoelektrotechnik, Speziell für Kryomagnete—Forschungsbericht*; Technical Report; Leichtmetall-Forschungsinstitut der Vereinigte Aluminum-Werke AG: Bonn, Germany, 1974.
37. Kim, S.; Reddy, R. Recent advances in electrodeposition technology. *J. Korean Inst. Surf. Eng.* **2001**, *34*, 553–567.
38. Wu, B.; Reddy, R.G.; Rogers, R.D. Aluminum Reduction via Near Room Temperature Electrolysis in Ionic Liquids BT. In *Essential Readings in Light Metals: Volume 2—Aluminum Reduction Technology*; Springer: Cham, Switzerland, 2016; pp. 1100–1106. [\[CrossRef\]](#)
39. Kurz, W.; Fisher, D.J. *Fundamentals of Solidification*, 3rd ed.; Trans Tech Publ.: Aedermannsdorf, Switzerland, 1989; pp. 53–55.
40. Weiser, K. Theoretical calculation of distribution coefficients of impurities in germanium and silicon, heats of solid solution. *J. Phys. Chem. Solids* **1958**, *7*, 118–126. [\[CrossRef\]](#)
41. Curtolo, D.; Friedrich, S.; Bellin, D.; Nayak, G.; Friedrich, B. Definition of a First Process Window for Purification of Aluminum via “Cooled Finger” Crystallization Technique. *Metals* **2017**, *7*, 341. [\[CrossRef\]](#)
42. Burton, J.A.; Prim, R.C.; Slichter, W.P. The distribution of solute in crystals grown from the melt. Part I. Theoretical. *J. Chem. Phys.* **1953**, *21*, 1987–1991. [\[CrossRef\]](#)
43. Drini, B.; Katgerman, L.; Boom, R. Metal refining with fractional crystallization: State-of-the-art and future prospects. In *Proceedings of the ECI Conference on Metal Separation Technologies III*; Aune, R.E., Kekkonen, M., Eds.; Helsinki University of Technology, Laboratory of Metallurgy: Espoo, Finland, 2004; pp. 34–41.
44. Dawless, R.K.; Graziano, R.E. Fractional Crystallization Process. U.S. Patent 4,294,612, 13 October 1994.
45. Jacobs, S.C.; Burrell, L. Purification of Aluminum. U.S. Patent 3,303,019, 7 February 1967.
46. Dawless, R.K.; Jacobs, S.C. Production of Extreme Purity Aluminum. U.S. Patent 4,273,627, 16 June 1981.
47. Kahveci, A.I.; Unal, A. Refining of a 5XXX series aluminum alloy scrap by alcoa fractional crystallization process. In *Proceedings of the Fourth International Symposium on Recycling of Metals and Engineered Materials*; Stewart, D.J., Daley, J., Stephens, R., Eds.; The Minerals, Metals & Materials Society: Pittsburgh, PA, USA, 2000; pp. 979–991.
48. De Vries, Paul, A.; Wouters, H.A. Method for Fractional Crystallization of a Molten Metal. Switzerland Patent 2004/005558A1, 30 December 2004.
49. Yang, G.; Govani, J.; Mei, H.; Guan, Y.; Wang, G.; Huang, M.; Mei, D. Investigation of influential factors on the purification of zone-refined germanium ingot. *Cryst. Res. Technol.* **2014**, *49*, 269–275. [\[CrossRef\]](#)
50. Spim, J.; Bernadou, M.; Garcia, A. Numerical modeling and optimization of zone refining. *J. Alloy. Compd.* **2000**, *298*, 299–305. [\[CrossRef\]](#)
51. Ghosh, K.; Mani, V.N.; Dhar, S. Numerical study and experimental investigation of zone refining in ultra-high purification of gallium and its use in the growth of GaAs epitaxial layers. *J. Cryst. Growth* **2009**, *311*, 1521–1528. [\[CrossRef\]](#)
52. Ho, C.D.; Yeh, H.M.; Yeh, T.L. Optimal zone lengths in multi-pass zone-refining processes. *Sep. Technol.* **1996**, *6*, 227–233. [\[CrossRef\]](#)
53. Ho, C.D.; Yeh, H.M.; Yeh, T.L. Simulation of multipass zone-refining processes. *Int. J. Model. Simul.* **2003**, *23*, 85–93. [\[CrossRef\]](#)
54. Yeh, H.M.; Yeh, W.H. The Improvement of Separation in Zone Refining Processes with Zone Length Varied along the Ingot. *Sep. Sci. Technol.* **1979**, *14*, 795–803. [\[CrossRef\]](#)
55. Pfann, W.G. *Zone Melting*; Wiley Series on the Science and Technology of Materials; John Wiley & Sons: New York, NY, USA; Chapman & Hall: London, UK, 1958.
56. Rodway, G.; Hunt, J. Optimizing zone refining. *J. Cryst. Growth* **1989**, *97*, 680–688. [\[CrossRef\]](#)
57. Prasad, D.S.; Munirathnam, N.R.; Rao, J.V.; Prakash, T.L. Effect of multi-pass, zone length and translation rate on impurity segregation during zone refining of tellurium. *Mater. Lett.* **2006**, *60*, 1875–1879. [\[CrossRef\]](#)
58. Kino, T.; Kamigaki, N.; Yamasaki, H.; Kawai, J.; Deguchi, Y.; Nakamichi, I. Zone refining of aluminum. *Trans. Jpn. Inst. Met.* **1976**, *17*, 645–648. [\[CrossRef\]](#)
59. Lee, H.Y.; Oh, J.K.; Lee, D.H. Purification of tin by zone refining with development of a new model. *Metall. Trans. B* **1990**, *21*, 455–461. [\[CrossRef\]](#)
60. Zhang, X.; Friedrich, S.; Friedrich, B. Production of High Purity Metals: A Review on Zone Refining Process. *J. Cryst. Process. Technol.* **2018**, *8*, 33–55. [\[CrossRef\]](#)
61. Tiller, W.; Jackson, K.; Rutter, J.; Chalmers, B. The redistribution of solute atoms during the solidification of metals. *Acta Metall.* **1953**, *1*, 428–437. [\[CrossRef\]](#)
62. Zaiour, A.; Hamdoun, B.; Charara, J.; Roumi, M.; Zahraman, K.; Hage-Ali, M. A New Theoretical Formulation of Temperature Effect on Impurities Diffusion Coefficients in Molten Tellurium. *Phys. Scr.* **2005**, *71*, 414–418. [\[CrossRef\]](#)

-
63. Munirathnam, N.R.; Prasad, D.S.; Sudheer, C.H.; Rao, J.V.; Prakash, T.L. Zone refining of cadmium and related characterization. *Bull. Mater. Sci.* **2005**, *28*, 209–212. [[CrossRef](#)]
 64. Liu, Y.C.; Moss, R.; Dost, S. A computational thermal analysis for the zone-refining processes of Cd and Te. *J. Cryst. Growth* **2006**, *293*, 146–156. [[CrossRef](#)]
 65. Kobayashi, N. Power required to form a floating zone and the zone shape. *J. Cryst. Growth* **1978**, *43*, 417–424. [[CrossRef](#)]
 66. Dost, S.; Liu, Y.C.; Haas, J.; Roszmann, J.; Grenier, S.; Audet, N. Effect of applied electric current on impurity transport in zone refining. *J. Cryst. Growth* **2007**, *307*, 211–218. [[CrossRef](#)]
 67. Hashimoto, E.; Ueda, Y. Zone refining of high-purity aluminum. *Mater. Trans. JIM* **1994**, *35*, 262–265. [[CrossRef](#)]
 68. Mikubo, S. The Latest Refining Technologies of Segregation Process to Produce high-purity aluminum. In Proceedings of the 12th International Conference on Aluminium Alloys, Yokohama, Japan, 5–9 September 2010; pp. 224–228.
 69. Ferber, M.E.; Winterberger, M.G. Process for Purification of Metals. U.S. Patent 3,671,229, 20 June 1972.
 70. Winterberger, M.G. Précédé de Purification de Métaux Per Ségrégation. France Patent 0091386A1, 12 October 1983.
 71. Shingu, H.; Arai, K.; Sakaguchi, M.; Nishide, T.; Watanabe, O.; Otsuka, R.; Tsukamoto, K. Process for Producing High-Purity Aluminum. U.S. Patent 4,469,512, 4 September 1984.
 72. Friedrich, S.; Coladetti Curtolo, D.; Friedrich, B. Effect of Process Parameter Variation on Purity during Rotary Fractional Crystallization of Aluminum. *Open J. Met.* **2017**, *7*, 25–38. [[CrossRef](#)]
 73. Hong, T.; Nurgul, I. Method for Purifying High-Purity Aluminum by Directional Solidification and Smelting Furnace Therefor. U.S. Patent 2014/0202653A1, 24 July 2014.